Chemical Physics Letters 629 (2015) 13–17

Contents lists available at ScienceDirect

Chemical Physics Letters

journal homepage: www.elsevier.com/locate/cplett

Quantum dots based broad spectral photodetectors with wavelength detecting ability

Fei Wang [a], Yunpeng Wang [a], Dongxu Zhao [a,*], Bin Zhao [a,b], Dengkui Wang [a,b]

[a] State Key Laboratory of Luminescence and Applications, Changchun Institute of Optics, Fine Mechanics and Physics, Chinese Academy of Sciences, 3888 Dongnanhu Road, Changchun 130021, People's Republic of China

[b] Graduate School of the Chinese Academy of Sciences, Beijing 100049, People's Republic of China

ARTICLE INFO

Article history:
Received 5 February 2015
In final form 9 April 2015
Available online 20 April 2015

ABSTRACT

Board spectral photodetectors are required for varied scientific and industrial applications, yet the studies of such devices are limited. In this work a CdSe/ZnS quantum dots (QDs) based photodetector with broad spectral detecting ability was fabricated through a simple approach. Due to the discrete electronic states of QDs, the photodetector was more sensitive to incident wavelengths than incident power densities, and the photocurrent decreased monotonously with increasing incident wavelength, which could also realize the wavelength detection of incident light. This character provides a new way to achieve color or image sensing, and it could also broaden the photodetection and photosensing applications of QDs and semiconductor detectors.

© 2015 Published by Elsevier B.V.

1. Introduction

Because of their insensitivity to magnetic fields, capability for high speed operation, good linearity and sensibility, semiconductor photodetectors are attracting increased attentions for potential applications in civil and military applications [1–8]. Yet most types of semiconductor photodetectors have the photoresponses only under a certain single wavelength or the light with a narrow range [9]. A photodetector with board spectral responses is required for broad applications including imaging, telecommunications, biomedicine, environmental monitoring and defence sensing [10–12]. In recent years, many efforts have been made to get broad spectral photodetectors by using small molecule materials [10], carbon nanotubes [11,13], narrow-bandgap semiconductor nanowires [9,14] and two-dimensional crystals [15] as functional layers. These devices have realized the wide response ranges, but the works that focus on the wavelength detecting abilities are limited. The relations between their responsivities and incident wavelengths are irregular [9–15], as a result, it is hard to predicate the incident wavelengths from the values of photocurrents, which has limited the color and image sensing applications of broad spectral photodetectors. A conventional way for photodetectors to achieve wavelength detecting is introducing absorptive filters in the device to get the red/green/blue response [16], but the filters require its own fabrication steps and meanwhile reduce the responsivities of the devices, a filter-free broad spectral detector with wavelength detecting ability is necessary. Because semiconductor quantum dots (QDs) have the quantum confinement effect of carriers in three-dimensionals, the electronic states will become completely discrete. As compared to continuous electronic states, the discrete electronic states will contribute to a regular and monotonous relation between photocurrent and incident wavelength, so using QDs as the active layer to fabricate photodetector will realize both broad spectral response and wavelength detecting ability. In this Letter, we designed a photodetector by using the colloidal CdSe QDs as functional layer, the surfaces of CdSe QDs were passivated by ZnS to improve its quantum yields [17] and enhance its quantum confinement effect [18]. We chose p-GaN and ZnO as p-type and n-type materials in the device because they all have wide band gaps and will not affect the photocurrent of QDs layer in the visible light region. Various strategies such as the self-assembled monolayer (SAM) method, Langmuir–Blodgett (LB) technique, layer-by-layer (LbL) assembly, exfoliation and synthetic techniques have been widely used for the preparations of semiconductor nanostructures or thin films [19,20]. For semiconductor QDs, the epitaxial growth method is hard to grow the QDs on large and flexible substrates [21]. For thin films, the metal organic chemical vapor deposition (MOCVD) and molecular beam epitaxy (MBE) equipments are very costly. Here in this work, solution processable colloidal QDs were synthesized by wet chemical methods, and the ZnO film was prepared by the simple sintering method. The detector was assembled through a simple but efficient approach on the

* Corresponding author. fax: +86 431 86176312.
E-mail address: zhaodx@ciomp.ac.cn (D. Zhao).

http://dx.doi.org/10.1016/j.cplett.2015.04.018
0009-2614/© 2015 Published by Elsevier B.V.

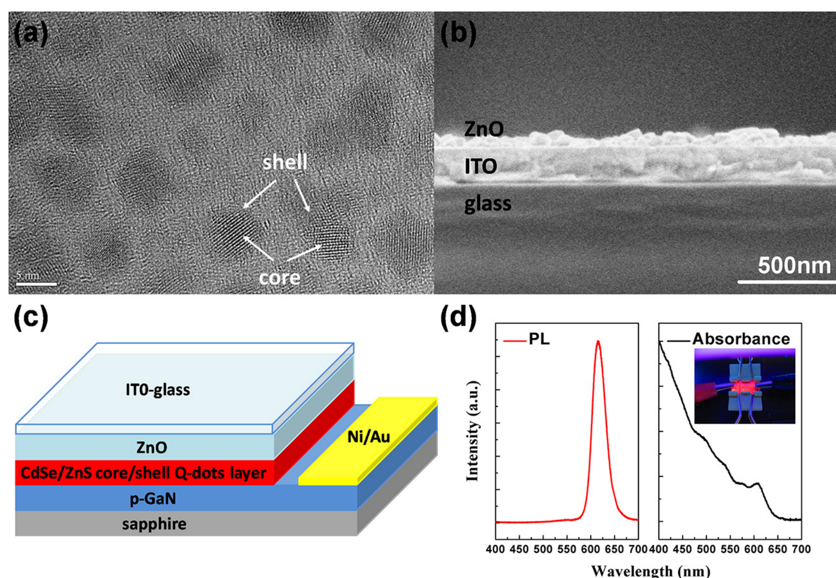

Figure 1. (a) HRTEM image of CdSe/ZnS core/shell QDs. (b) Cross-sectional SEM image of ZnO layer fabricated on ITO-glass. (c) Schematic configuration of the photodetector. (d) Room-temperature PL and the optical absorption spectra of the QDs. Insert is a photograph of the device under UV illumination.

basis of as-prepared materials, then broad spectral response and wavelength detection were observed.

2. Experimental methods

CdSe/ZnS core/shell QDs used in this work were synthetized by a two-step chemical method mentioned elsewhere [17]. The p-GaN thin film on sapphire substrate was prepared by MOCVD method. The Ni/Au contact on the GaN substrate was deposited by thermal evaporation method. The ZnO thin film used in this experiment was fabricated by a simple sintering method with following steps: First, ITO-glass substrates were cut into pieces of 1 cm × 1 cm, and strictly ultrasonic cleaned in acetone, ethanol and deionized water separately, 15 min for each. Then, zinc acetate ($Zn(CH_3COO)_2$) was dissolved in ethanol to form a solution with the concentration of 30 mg/ml. The zinc acetate solution was spin-coated on ITO glass substrates. Then the substrates were sintered at 400 °C in the tube furnace for 20 min. The process of spin-coating and sintering was repeated four times. The QDs based photodetector was fabricated as the following step: first, the ZnO coated ITO-glass and GaN thin film were clamped tightly by a binder clip. Then, the QDs solution was doped into the gap between ZnO and GaN layers. Due to the capillary action of liquid [22,23], the QDs solution formed a uniform layer between ZnO and GaN layers. Finally, the device was dried at 60 °C for 24 h to volatilize all the organic solvent, then the fabrication of the device was done.

The high resolution transmission electron microscope (HRTEM) in this work was obtained on a JEOL JEM-2100 F equipment. The morphology of samples was investigated by the field-emission scanning electron microscopy (FESEM, Hitachi S-4800). The photoluminescence (PL) measurement was carried out with a JY-630 micro-Raman spectrometer by using the 325 nm line of a He–Cd laser as the excitation source, and the absorption spectra were carried out using a Shimadzu UV-3101 PC spectrophotometer. The typical *I–V* curves were measured by a keithley 2611A measurement, and the time-resolved photo-current testing were carried out by using an optical chopper (EG&G 192) to turn on and turn off the light that illuminated on the device and using the 2611A measurement to record the time and corresponding photocurrent values. Commercial LEDs (400 nm, 470 nm) and UV lamp (365 nm) were served as light sources to carry out the *I–V* and time-resolved photocurrent characteristics of the device. To test the broad spectral detecting ability of the device, a monochromator (Shimadzu RF-520) equipped with a 150 W Xe lamp were served as light source to measure the responsivities and external quantum efficiencies under different wavelengths. The power densities of all driven light were evaluated by Ophir PD300R-UV power meter and calibrated by adjusting the applied bias to achieve a similar intensity to the UV lamp.

3. Results and discussion

Figure 1(a) shows the HRTEM image of the QDs, the CdSe single crystal core and the ZnS shell could be observed clearly in the picture. The average diameter of the QDs is about 5 nm. Figure 1(b) shows the FESEM image of the ZnO thin film that was sintered on the ITO glass. The thin film is consisted of ZnO crystal grains and the thickness of this film is about 50–60 nm. As can be seen in Figure S1, the photoluminescence (PL) peak of ZnO layer is located at 370 nm and the first exciton absorption peak of the film is centered at 360 nm. Figure 1(c) is the schematic description of the detector's sandwich structure, we use p-GaN and ZnO as p-type and n-type materials and the upper ITO-glass side is the light entrance side of the detector. Figure S2 shows the PL spectrum of p-GaN thin film used in this work, and the spectrum consists of two parts: NBE emission centered at 361 nm and a defective emission peak located at 377 nm. Figure 1(d) shows the PL spectrum and the optical absorption spectrum of QDs, the emission peak and the absorption edge of the CdSe/ZnS core/shell QDs are all located at about 625 nm. The insert of Figure 1(d) is a photograph of the detector under UV illumination. The uniform red color covering the whole device was originated from the photoluminescence of QDs layer, which means the QDs thin film was wholly and uniformly applied into the device by the method mentioned in this work.

Supplementary data associated with this article can be found, in the online version, at doi:10.1016/j.cplett.2015.04.018

Figure 2 shows the typical *I–V* characteristics of the detector in dark and under the illumination of 400 nm light. When in the dark, the *I–V* curve shows that the detector behaves like an efficient diode with a current increasing rapidly under forward bias and blocking the current flow under reverse bias, which indicates the ZnO thin film fabricated in this work has good electrical

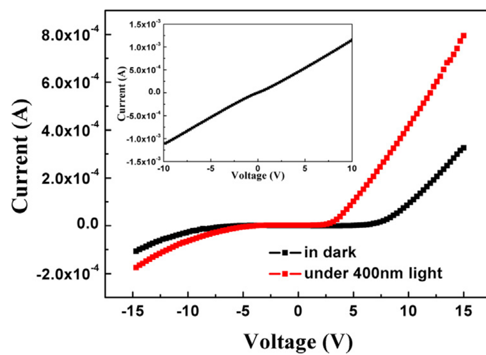

Figure 2. Typical *I–V* characteristics of the sample, insert presents the *I–V* curve between two Ni/Au contacts on the p-GaN substrate.

properties. The threshold voltage of the device is about 7 V. But when under 400 nm light illumination, the photo-induced carriers in QDs will reduce the resistance of QDs layer, the conductive QDs layer acts as an n-type material in the device and the barrier between p-GaN and ZnO is reduced. As a result, the reverse bias blocking is eased and the turn on voltage reduces to about 3 V, which means the QDs has played the role of functional layer in the device. The insert of Figure 2 implies that the contact between Ni/Au electrode and p-GaN film is ohmic.

For testing the broad spectral detecting ability of the device, a monochromator equipped with a Xe lamp were served as light source. As a critical parameter to characterize the performance of photodetectors, the responsivity can be expressed as $R_\lambda = \Delta I/(AP)$, where ΔI is the photocurrent difference between the dark and illumination, A is the contact area and P is the irradiance of light source under different wavelengths. Herein, $A = 0.5\ \text{cm} \times 0.5\ \text{cm} = 0.25\ \text{cm}^2$, the responsivity and external quantum efficiency (EQE) of the device under the bias of −15 V was calculated and shown in Figure 3(a). For understanding the role of the QDs layer in device clearly, we fabricated a device by the same method but without the QDs layer for the reference. When there is no QDs layer, the device only have a low response peak located at 370 nm caused by the photoresponse of ZnO and GaN. Figure 3(b) is the time-resolved photocurrent curves of the device, we could see a weak response under the illumination of 365 nm, and there is no obvious response under other wavelengths. After we introduced the QDs layer in the detector, the resistance of the device has increased and the dark current has decreased correspondingly. The device presents a wide spectral response in accord with the range of absorption spectrum showed in Figure 1(d). The responsivity and EQE of the device could reach up to 400 mA/W and 135%. The response range and responsivity of the device are both enhanced as compared to previously reported results of ZnO/GaN heterojunction photodetectors [24,25]. As shown in Figure 3(c), the device with the QDs layer presents a good response ability. When under different incident lights, the values of photocurrent change greatly and the photocurrent increases monotonically with the decreasing of incident wavelengths, which is in line with the spectral response curve of the device. The photocurrent values in Figure 3(c) are approximately matched with the photocurrent values in Figure 3(a), which confirms the QDs layer plays the main role in the photoresponse, and the detector could be used in wavelength detecting application. We use a nonlinear fitting program to work out the response time of the device, and the biexponential equation is shown as following

$$I = I_0 + Ae^{-t/\tau_1} + Be^{-t/\tau_2} \qquad (1)$$

where I, I_0, A, B are the fitting parameters, τ_1 and τ_2 are the fast and slow time constants [26–28]. The corresponding fitted curves are shown in Figure 4(a), the response time $\tau_{on,1}$ is 0.05 s, $\tau_{on,2}$ is 2.80 s

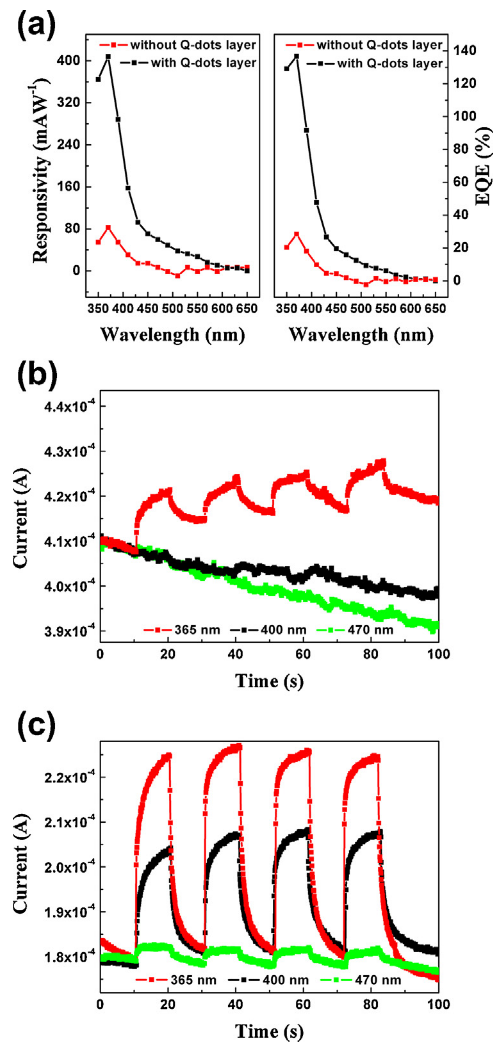

Figure 3. (a) Responsivity and EQE curves of the devices with and without the quantum dots layer under different wavelengths. (b) Time-resolved photocurrent of the device without the quantum dots layer in response of 365 nm light. (c) Time-resolved photocurrent of the device with the quantum dots layer in response of different wavelength light.

and the recovery times $\tau_{off,1}$, $\tau_{off,2}$ are 0.29 s and 2.56 s. The fast time constants are due to the trapping at the surface states and the slow time constants can be attributed to a carrier relaxation process in the deep defect states [26–28]. The device without QDs layer has the same response time in Figure 3(b). Figure 4(b) shows the detecting mechanism of the device. When a reverse bias is applied on the device, there will be a wide depletion region that appears at the interface between p-GaN and ZnO. The charges in depletion region lead to a built-in electric field E_{bi}. As soon as the QDs layer absorbs a photon, an electron–hole pair is generated, under the effect of E_{bi}, the photo-generated carriers will be separated quickly, then the electrons transfer to the ITO-glass and the holes transfer to the Ni/Au electrode, which results in an increase of the current, and the detecting speed is attributed to the built-in electric field too.

We have discussed the relation between photocurrent values and incident wavelengths above, but the power density of incident light could also change the photocurrent value of the device. For a wavelength detecting device, the influence of incident power densities should be eliminated. So we have investigated the effects of incident power density on the photocurrent value of the device. Figure 5 is time-resolved photocurrent of the device under 400 nm illumination with different power densities. As shown in

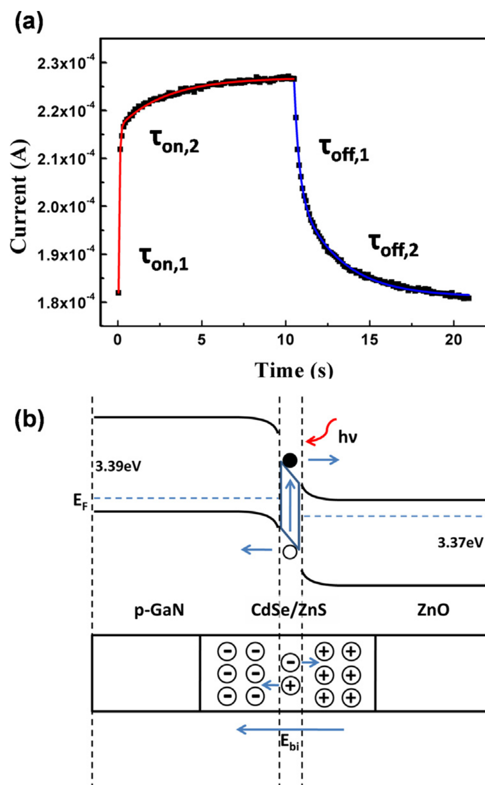

Figure 4. (a) Time-resolved photocurrent under 365 nm light at the applied bias of −15 V and the biexponential fitting curve. (b) The energy band diagram of the photodetector under reverse bias.

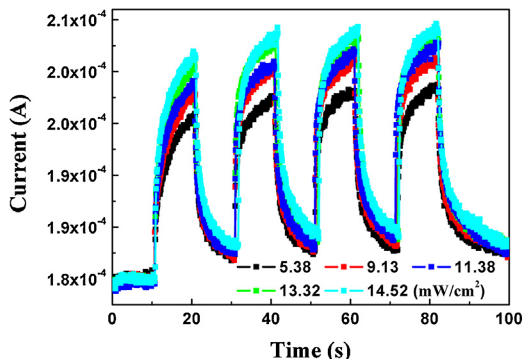

Figure 5. Time-resolved photocurrent of the device under 400 nm light with different power densities.

the figure, the incident power density changes from 5.38 mW/cm^2 to 14.52 mW/cm^2, but the photocurrent of the device doesn't change much as compared to varying the incident wavelengths in Figure 3(c). It can be explained by the quantum confinement effect of QDs. When light illuminates on the photodetector, higher incidence power density means more photons, so under the condition of continuous electronic state, more incident photons could excite more carriers. That is why the photocurrent is sensitive to the power density of incidence light as the results reported by previous research [1,9,15]. But in QDs, the electronic states become completely discrete as in atoms and molecules [29–32]. Because electrons are fermions, considering the Pauli exclusion principle (no two identical electrons may occupy the same quantum state simultaneously), more photons cannot excite the electrons to higher energy levels to form electron−hole pairs in QDs except increasing the photon energy. Hence, the photocurrent change of the device is small when the power density of incident light increased by several times, but it is much bigger when the wavelength of incident light changed. QDs based photodetector is more sensitive to the wavelength of incidence light than the power density, so it is an appropriate approach to realize the wavelength detecting.

The p-GaN and n-ZnO are difficult to be processed in solution. Also, it is hard to achieve high-quality thin films on the QDs coated substrates. So in previous works, most of QDs photodetectors were symmetrical structured photoconductive detectors [33–36]. Due to the crystal boundaries among QDs, the photoconductive detectors have been suffering the low photocurrent of about 10^{-7} A [35,36], which has limited the improvements of device performances. In this work, by using the clamping and dropping method, we have uniformly applied the colloidal QDs between ZnO and GaN layers. The device has the sandwich geometry, and the GaN, QDs and ZnO materials were served as p/i/n layers respectively in the detector. The photocurrent of the detector has increased to 10^{-4} A. The method mentioned here could be utilized to fabricate other sandwich structured photoelectric devices of semiconductor thin films.

4. Conclusion

In conclusion, a CdSe/ZnS QDs based photodetector have been fabricated through a simple but efficient approach. The detector presented good *I*–*V* characteristics and reversible photoresponses. The responsivity of the device could reach up to 400 mA/W. Most importantly, the device had a broad light detection range in accordance with the absorption spectrum of the QDs layer. Because of the discrete electronic states of QDs, the photodetector was more sensitive to incident wavelengths than incident power densities, and the photocurrent decreased monotonously with increasing incident wavelength, which is in line with the spectral response curve of the device under different incident wavelengths. This kind of photodetector has realized the wavelength detection of incident light, and it also provides a new way to achieve color and image sensing applications.

Acknowledgments

This work is supported by National Basic Research Program of China (973 Program) under Grant No. 2011CB302004, the Key Program of National Natural Science Foundation of China under Grant No. 11134009, the National Natural Science Foundation of China under Grant No. 21101146.

References

[1] E. Monroy, F. Omnes, F. Calle, Semicond. Sci. Technol. 18 (2003) R33.
[2] W. Yang, R.D. Vispute, S. Choopun, R.P. Sharma, Appl. Phys. Lett. 78 (2001) 2787.
[3] D.Y. Jiang, J.Y. Zhang, Y.M. Lu, K.W. Liu, D.X. Zhao, Z.Z. Zhang, D.Z. Shen, X.W. Fan, Solid-State Electron. 52 (2008) 679.
[4] Z. Guo, D.X. Zhao, Y.C. Liu, D.Z. Shen, J.Y. Zhang, B.H. Li, Appl. Phys. Lett. 93 (2008) 163501.
[5] C. Soci, A. Zhang, B. Xiang, S.A. Dayeh, D.P.R. Aplin, J. Park, X.Y. Bao, Y.H. Lo, D. Wang, Nano Lett. 7 (2007) 1003.
[6] L.W. Ji, S.M. Peng, Y.K. Su, S.J. Young, C.Z. Wu, W.B. Cheng, Appl. Phys. Lett. 94 (2009) 203106.
[7] X. Fang, S. Xiong, T. Zhai, Y. Bando, M. Liao, U.K. Gautam, Y. Koide, X. Zhang, Y. Qian, D. Golberg, Adv. Mater. 21 (2009) 5016.
[8] Y. Yang, W. Guo, J. Qi, J. Zhao, Y. Zhang, Appl. Phys. Lett. 97 (2010) 223113.
[9] Z. Wang, M. Safdar, C. Jiang, J. He, Nano Lett. 12 (2012) 4715.
[10] S.H. Wu, W.L. Li, B. Chu, Z.S. Su, F. Zhang, C.S. Lee, Appl. Phys. Lett. 99 (2011) 023305.
[11] M.S. Arnold, J.D. Zimmerman, C.K. Renshaw, X. Xu, R.R. Lunt, C.M. Austin, S.R. Forrest, Nano Lett. 9 (2009) 3354.
[12] R. Dong, C. Bi, Q. Dong, F. Guo, Y. Yuan, Y. Fang, Z. Xiao, J. Huang, Adv. Opt. Mater. 2 (2014) 549.
[13] Y. Xie, M. Gong, T.A. Shastry, J. Lohrman, M.C. Hersam, H. Ren, Adv. Mater. 25 (2013) 3433.
[14] B. Chen, J. Xu, Z. Ouyang, X. Su, Y. Xiao, S. Lei, J. Mater. Chem. C 2 (2014) 1808.

[15] S.R. Tamalampudi, Y.Y. Lu, U.R. Kumar, R. Sankar, C.D. Liao, B.K. Moorthy, C.H. Cheng, Chou F.C., Y. Chen, Nano Lett 14 (2014) 2800.
[16] H. Park, Y. Dan, K. Seo, Y.J. Yu, P.K. Duane, M. Wober, K.B. Crozier, Nano Lett. 14 (2014) 1804.
[17] B.O. Dabbousi, J. Rodriguez-Viejo, F.V. Mikulec, J.R. Heine, H. Mattoussi, R. Ober, K.F. Jensen, M.G. Bawendi, J. Phys. Chem. B 101 (1997) 9463.
[18] S. Kim, B. Fisher, H.J. Eisler, M. Bawendi, J. Am. Chem. Soc. 125 (2003) 11466.
[19] D. Jariwala, V.K. Sangwan, L.J. Lauhon, T.J. Marks, M.C. Hersam, ACS Nano 8 (2014) 1102.
[20] K. Ariga, Y. Yamauchi, G. Rydzek, Q. Ji, Y. Yonamine, K.C.W. Wu, J.P. Hill, Chem. Lett. 43 (2014) 36.
[21] D.C. Oertel, M.G. Bawendi, A.C. Arango, V. Bulović, Appl. Phys. Lett. 87 (2005) 213505.
[22] E.W. Washburn, Phys. Rev. 17 (1921) 273.
[23] L.A. Richards, Physics 1 (1931) 318.
[24] L. Su, Q. Zhang, T. Wu, M. Chen, Y. Su, Y. Zhu, R. Xiang, X. Gui, Z. Tang, Appl. Phys. Lett. 105 (2014) 072106.
[25] H. Zhu, C.X. Shan, B. Yao, B.H. Li, J.Y. Zhang, D.X. Zhao, D.Z. Shen, X.W. Fan, J. Phys. Chem. C 112 (2008) 20546.
[26] A. Bera, D. Basak, Appl. Phys. Lett. 93 (2008) 053102.
[27] S.E. Ahn, J.S. Lee, H. Kim, S. Kim, B.H. Kang, K.H. Kim, G.T. Kim, Appl. Phys. Lett. 84 (2004) 5022.
[28] W. Yan, N. Mechau, H. Hahn, R. Krupke, Nanotechnology 21 (2010) 115501.
[29] N.F. Borrelli, D.W. Hall, H.J. Holland, D.W. Smith, J. Appl. Phys. 61 (1987) 5399.
[30] T. Takagahara, Phys. Rev. B 47 (1993) 4569.
[31] W.L. Wilson, P.F. Szajowski, L.E. Brus, Science 262 (1993) 1242.
[32] T. Takagahara, K. Takeda, Phys. Rev. B 46 (1992) 15578.
[33] S. Keuleyan, E. Lhuillier, V. Brajuskovic, P.G. Sionnest, Nat. Photon 5 (2011) 489.
[34] D.Y. Guo, C.X. Shan, S.N. Qu, D.Z. Shen, Sci. Rep. 4 (2014) 7469.
[35] M. Chen, H. Yu, S.V. Kershaw, H. Xu, S. Gupta, F. Hetsch, A.L. Rogach, N. Zhao, Adv. Funct. Mater. 24 (2014) 53.
[36] D. Kufer, I. Nikitskiy, T. Lasanta, G. Navickaite, F.H.L. Koppens, G. Konstantatos, Adv. Mater. 27 (2015) 176.